

**Lattice dynamics in monolayer and few-layer SnSe<sub>2</sub>**Wei Zhou,<sup>1,2,\*</sup> Zhenhai Yu,<sup>3</sup> Hao Song,<sup>1</sup> Ruiyang Fang,<sup>1</sup> Zhangting Wu,<sup>4</sup> Ling Li,<sup>1</sup> Zhenhua Ni,<sup>4</sup>  
Wei Ren,<sup>5</sup> Lin Wang,<sup>3</sup> and Shuangchen Ruan<sup>1,†</sup><sup>1</sup>Shenzhen Key Laboratory of Laser Engineering, College of Optoelectronic Engineering, Shenzhen University, Shenzhen 518060, China<sup>2</sup>National Laboratory of Solid State Microstructures, School of Physics, Collaborative Innovation Center of Advanced Microstructures, Nanjing University, Nanjing 210093, China<sup>3</sup>Center for High Pressure Science and Technology Advanced Research, Shanghai 201203, China<sup>4</sup>Department of Physics, Southeast University, Nanjing 211189, China<sup>5</sup>International Centre for Quantum and Molecular Structures, Department of Physics, Materials Genome Institute and Shanghai Key Laboratory of High Temperature Superconductors, Shanghai University, Shanghai 200444, China

(Received 21 January 2017; published 5 July 2017)

Hexagonal tin diselenide (6Hb-SnSe<sub>2</sub>), a two-dimensional (2D) layered metal dichalcogenide from the IVA and VIA groups, has recently drawn numerous attention in 2D nano-optoelectronics. In this paper, we investigate characteristic lattice dynamics of mechanically exfoliated mono- and few-layer 6Hb-SnSe<sub>2</sub> samples by Raman spectroscopy. Bulk SnSe<sub>2</sub> has all four Raman active modes of low-frequency shear  $E_g^2$  and layer-breathing  $A_{1g}^2$  modes, and high-frequency intralayer vibrational  $E_g^1$  and  $A_{1g}^1$  modes observed around 18.9, 33.6, 107.9, and 182.1 cm<sup>-1</sup>, respectively. From polarized Raman measurements, we find that  $E_g^1$  mode intensity is independent of polarization configuration and increases linearly with layer number, which provides an effective approach to determine sample thickness. From low-temperature Raman measurements,  $E_g^1$  and  $A_{1g}^1$  mode temperature coefficients of one-layer, three-layer, and bulk SnSe<sub>2</sub> are around -0.018 and -0.014 cm<sup>-1</sup>/K, whereas they have almost zero values for low-frequency  $E_g^2$  and  $A_{1g}^2$  modes of bulk SnSe<sub>2</sub> due to different thermal responses of intralayer and interlayer vibrations. Using multiple excitation laser lines of 488, 514.5, 568, 647, and 785 nm,  $E_g^1$  and  $A_{1g}^1$  mode intensities of bulk SnSe<sub>2</sub> have a similar trend with weak maxima around 2.41 eV. Our work provides valuable information about SnSe<sub>2</sub> lattice vibrations for further fundamental research and potential applications in 2D devices such as thermoelectric and infrared light detectors.

DOI: [10.1103/PhysRevB.96.035401](https://doi.org/10.1103/PhysRevB.96.035401)**I. INTRODUCTION**

After the discovery of graphene and its novel transport properties [1–3], layered transition-metal dichalcogenides (TMDCs) have attracted tremendous interest recently due to their rich physics and wide two-dimensional (2D) device applications. Semiconductor 2H-TMDCs are typically composed of layered  $MX_2$  structure, with  $M$  as transitional-metal elements (e.g., Mo and W) and  $X$  as chalcogenides (S, Se, and Te). Perpendicular to the covalently bonded  $X-M-X$  trilayer, the weak interlayer van der Waals (vdW) bonding enables exfoliation of TMDCs down to a monolayer. Furthermore, other layered TMDCs including ReS<sub>2</sub> and ReSe<sub>2</sub> possess different crystal structures of lower symmetry and strong in-plane anisotropy. Atomically thin TMDCs have novel properties such as direct band gaps in visible and near-infrared regions, relatively high carrier mobility up to 100 cm<sup>2</sup> V<sup>-1</sup> s<sup>-1</sup>, and coupled spin-valley degrees of freedom. These properties lead to intense investigation of TMDCs in optoelectronics for high-efficiency solar cells, broadband photodetectors up to the infrared range, and electronics for high-performance field-effect transistors and spin valleytronics [4–8].

Different from TMDCs, hexagonal tin diselenide (6Hb-SnSe<sub>2</sub>) has metal Sn atoms replacing the transitional-metal W and Mo atoms, making it a similar but quite different semiconductor with unique thermal, electronic, and optical

properties. The group-IV element Sn has outer  $p$  electrons rather than  $d$  electrons of Mo involved in the structural bonding, leading to the indirect semiconductor nature of SnSe<sub>2</sub> with a smaller band gap around 1 eV and weak photoluminescence which is hardly observable [9]. As a promising 2D material, SnSe<sub>2</sub> has been recently investigated as a thermoelectric material comparable to Bi<sub>2</sub>Te<sub>3</sub> and Bi<sub>2</sub>Se<sub>3</sub> [10,11], field-effect transistors [12–14], tunneling field-effect transistors [15], phase change memory material [16,17], and high-performance fast photodetectors [18,19] as reviewed in [20]. Furthermore, SnSe<sub>2</sub> has added new functions into vdW heterostructures such as Esaki diodes by introducing the type-III broken gap band alignment between SnSe<sub>2</sub> and black phosphorus [21].

With increasing interest in SnSe<sub>2</sub> in optoelectronics, theoretical [22] and experimental investigation of its layer-dependent optical, vibrational, and thermal properties are few. In recent Raman investigation of SnSe<sub>2</sub> nanosheets and bulk samples, temperature and pressure coefficients of the out-of-plane  $A_{1g}^1$  mode were obtained [23,24]. However, the characteristic in-plane  $E_g^1$  mode was absent. Furthermore, there was no similar phase transition of MoS<sub>2</sub> observed under hydrostatic pressure. We attribute these discrepancies to sample quality and the relative weak  $E_g^1$  mode. Mechanically exfoliated SnSe<sub>2</sub> flakes are high-quality single crystals; the important in-plane vibration information can be easier to access.

In this work, we report a systematical investigation of lattice vibrations of mechanically exfoliated mono- to few-layer SnSe<sub>2</sub> samples by Raman spectroscopy. For bulk SnSe<sub>2</sub>, we observe all four characteristic Raman modes,  $E_g^2$ ,  $A_{1g}^2$ ,  $E_g^1$ , and  $A_{1g}^1$ , around 18.9, 33.6, 107.9, and 182.1 cm<sup>-1</sup>.

\*wzhou@szu.edu.cn

†sruan@szu.edu.cn

Polarized Raman measurements show two in-plane  $E$  modes are polarization insensitive, and the linear thickness dependence of  $E_g^1$  mode intensity is useful to determine the SnSe<sub>2</sub> layer number. We further investigate one-layer, three-layer, and bulk SnSe<sub>2</sub> lattice vibrations at a temperature range of 77–300 K. Temperature coefficients of SnSe<sub>2</sub>  $E_g^1$  and  $A_{1g}^1$  modes are around  $-0.018$  and  $-0.014$   $\text{cm}^{-1}/\text{K}$ , similar to those of MoS<sub>2</sub>. However, low-frequency  $E_g^2$  and  $A_{1g}^2$  Raman shifts and full width at half maximum (FWHM) have almost no temperature dependence. Finally, to check electronic states involved in phonon scattering, we perform Raman measurements of bulk SnSe<sub>2</sub> using multiple incident lasers;  $E_g^1$  and  $A_{1g}^1$  modes are both nondispersive, with the same intensity resonances for a 2.41-eV laser, which can be from interband transitions.

## II. EXPERIMENT

One- to three-layer (1–3L) 6Hb-SnSe<sub>2</sub> samples are obtained by mechanical exfoliation of bulk single-crystal SnSe<sub>2</sub> (2D semiconductors) onto Si substrates of 300-nm SiO<sub>2</sub>. SnSe<sub>2</sub> flakes are first identified under a Zeiss optical microscope; then an atomic force microscope (AFM, Bruker) using the ScanAsyst mode is used to measure sample thickness. Raman measurements are conducted on a Horiba-JY T64000 system using backscattering geometry; the incident laser wavelength is 514.5 nm with spot size about  $2 \mu\text{m}$  in diameter. Laser power is kept as low as 0.1 mW to minimize the heating damage. For low-frequency polarized Raman experiments, the Horiba low-frequency Raman suite is used. The incident laser polarization direction is parallel to the polarizer initially; then we use a half wave plate to rotate the incident laser polarization by  $10^\circ$  for every spectrum. For low-temperature Raman experiments, a Linkam stage lowers the temperature from 300 to 77 K before measurements, and a vacuum pump keeps sample surfaces clean from ice. We use multiple linear laser lines of 488, 514, 568, 647, and 785 nm to investigate  $E_g^1$  and  $A_{1g}^1$  modes of bulk SnSe<sub>2</sub>. To avoid the influence from laser polarization, all five incident lasers are polarized in the same [010] direction and focused on the same sample spot [25]. Raman shifts and FWHM are obtained by the Lorentzian fitting procedure.

## III. RESULTS AND DISCUSSION

Figure 1(a) shows the optical image of one exfoliated SnSe<sub>2</sub> flake on the SiO<sub>2</sub>/Si substrate; the thicknesses of different parts are measured by AFM with the corresponding height profiles in Fig. 1(b). The ideal height value of monolayer SnSe<sub>2</sub> is 0.62 nm [26]. At ambient conditions, a larger value of 1.2 nm is reasonable for monolayer SnSe<sub>2</sub> due to possible influences from environments such as substrate smoothness, absorbed molecules, and AFM measurement errors. Recently, a close height value of 0.87 nm has been obtained for monolayer SnSe<sub>2</sub> [19] and 1.0 nm for SnS<sub>2</sub> monolayer [27].

Composed of three Se-Sn-Se trilayer repeats, 6Hb-SnSe<sub>2</sub> has its symmetry characterized by the space group  $D_{3d}^3(P\bar{3}m1)$ , whose 27 normal modes contain Raman active modes  $4A_{1g}$  and  $4E_g$  [28]. In Fig. 1(c), we present Raman spectra of few-layer SnSe<sub>2</sub> samples above  $100 \text{ cm}^{-1}$ ; in-plane  $E_g^1$  and out-of-plane  $A_{1g}^1$  modes are both obtained around 108.1

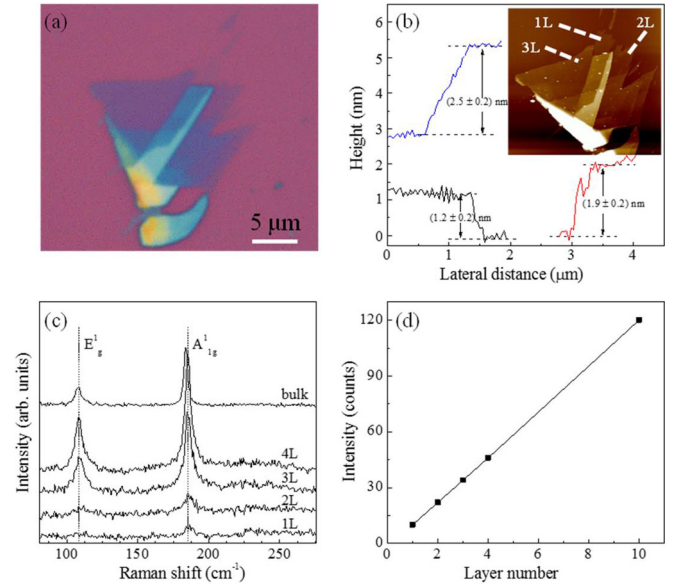


FIG. 1. (a) The optical image of one SnSe<sub>2</sub> flake with 1L, 2L, and 3L parts. (b) AFM height profiles of 1L (black), 2L (red), and 3L (blue) SnSe<sub>2</sub> along white line directions of the inserted AFM image. (c) Raman spectra of 1–4L and bulk SnSe<sub>2</sub>; the vertical dashed lines are a guide for the eyes. (d) SnSe<sub>2</sub>  $E_g^1$  mode intensity with respect to layer number.

and  $185.2 \text{ cm}^{-1}$ , similar to previous reports [28,29]. Due to weak intensities of  $E_g^1$  and  $A_{1g}^1$  modes of 1–2L SnSe<sub>2</sub> samples, we observe no clear thickness dependence of Raman frequency within the experimental error bar, similar to the “monolayer” behavior of ReS<sub>2</sub> [30]. Compared with few-layer SnSe<sub>2</sub>, bulk SnSe<sub>2</sub> the  $E_g^1$  mode has almost no shift and the  $A_{1g}^1$  mode

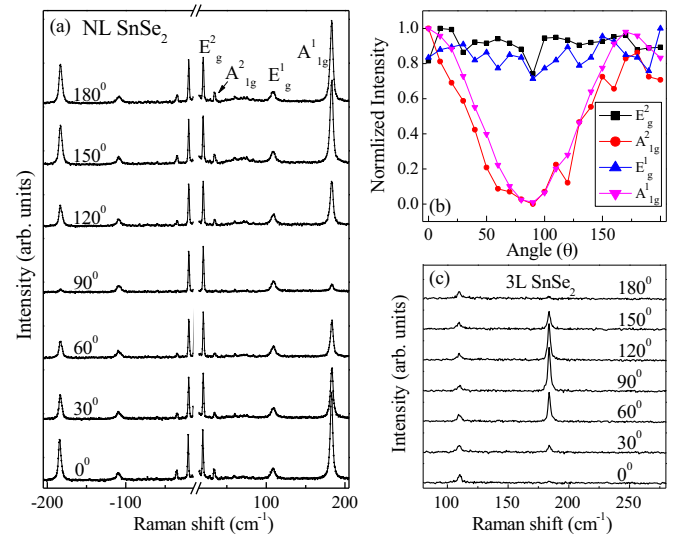


FIG. 2. (a) Low-frequency Raman spectra of NL SnSe<sub>2</sub> for selected rotated laser polarization angles  $\theta$  from the initial parallel polarized configuration. (b) Normalized  $E_g^2$  (black squares),  $A_{1g}^2$  (red circles),  $E_g^1$  (blue upward triangles), and  $A_{1g}^1$  (magenta downward triangles) mode intensities of NL SnSe<sub>2</sub> with respect to angle  $\theta$ . (c) Raman spectra of 3L SnSe<sub>2</sub> for selected angle  $\theta$ .

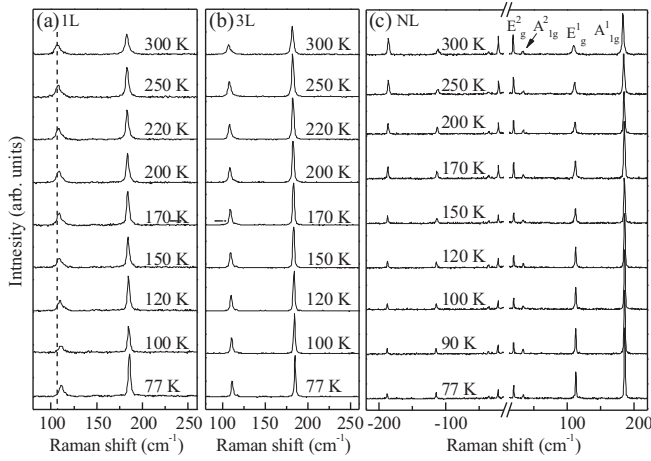


FIG. 3. (a–c) 1L, 3L, and bulk SnSe<sub>2</sub> Raman spectra of selected temperatures from 77 to 300 K; the vertical dotted line in (a) is a guide for the eye. Spectra are shifted vertically for clarity.

saturates around 184.1 cm<sup>-1</sup>, indicating the A<sub>1g</sub><sup>1</sup> mode frequency redshifts with respect to increasing layer number. This behavior is also quite different from that of MoS<sub>2</sub>, where E<sub>2g</sub><sup>1</sup> and A<sub>1g</sub><sup>1</sup> modes redshift and blueshift, respectively with increasing layer number. The Raman frequency trend of 2H-TMDCs such as MoS<sub>2</sub> [31] and MoTe<sub>2</sub> [32] can be ascribed to surface effects and inter- and intralayer couplings. Whereas 1T'-TMDCs including ReS<sub>2</sub> and ReSe<sub>2</sub> have comparable interlayer couplings with 2H-TMDCs, their layer-breathing and shear modes have different frequency trends and can be rationalized by symmetry arguments [33].

SnSe<sub>2</sub> Raman mode frequency shift trends are different from those of 2H-TMDC MoS<sub>2</sub>; the underlying mechanism including thickness and surface effects deserves further experimental and theoretical investigation.

As shown in Fig. 1(d), E<sub>g</sub><sup>1</sup> mode intensity of SnSe<sub>2</sub> increases almost linearly for 1–4L samples; showing the increased sample amount effect, similar behavior has been used to determine SnSe<sub>2</sub> and SnS<sub>2</sub> sample thickness recently [19,27]. For thicker samples, we observed E<sub>g</sub><sup>1</sup> mode intensity is not necessarily increased and can be even weaker than few-layer samples due to the interference effect. From experimental and theoretical simulation of MoS<sub>2</sub> interference effect [34], Raman mode intensity increases with sample thickness until reaching a critical thickness depending on optical environments such as substrates and lasers. To explore 2D effects, 1L to few-layer samples can be determined empirically using this linear relation. Considering measured Raman mode intensity depends on many factors including laser power, focusing, integration time, etc., Raman spectroscopy provides a proper method to determine the relative rather than absolute sample thickness. Furthermore, lasers used in Raman experiments are generally linearly polarized, whereas SnSe<sub>2</sub> Raman modes and the Si characteristic Raman mode around 520.7 cm<sup>-1</sup> can be polarization sensitive. To use intensity ratios of E<sub>g</sub><sup>1</sup> and A<sub>1g</sub><sup>1</sup> modes over Si 520.7 cm<sup>-1</sup> mode as a proper approach to determine SnSe<sub>2</sub> sample thickness, the polarization configuration should be specified and fixed during measurements, and the Raman mode symmetry should be understood.

We then check the symmetry of Raman modes by low-frequency polarized Raman experiments down to 15 cm<sup>-1</sup>. At ambient conditions, the linear 514.5-nm laser of 0.1 mW

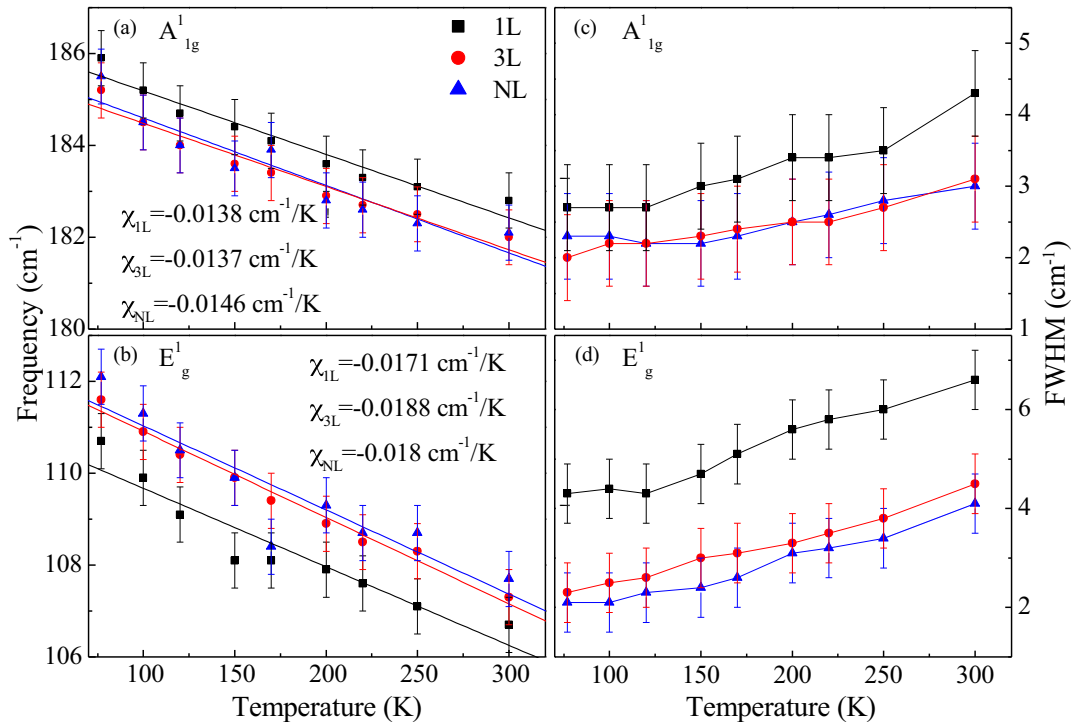


FIG. 4. Raman shifts of (a) A<sub>1g</sub><sup>1</sup> and (b) E<sub>g</sub><sup>1</sup> modes with respect to temperature for 1L (black squares), 3L (red circles), and bulk (blue triangles) SnSe<sub>2</sub> samples. The three solid lines are linear fittings of data. The corresponding FWHM of A<sub>1g</sub><sup>1</sup> and E<sub>g</sub><sup>1</sup> modes are presented in (c,d), respectively, where three lines connecting data points are a guide for the eye.

is focused on the 2D plane of bulk SnSe<sub>2</sub>. Selected Raman spectra of the bulk SnSe<sub>2</sub> sample are shown in Fig. 2(a). Symmetric Stokes and anti-Stokes modes can be identified as  $E_g^2$  (18.9 cm<sup>-1</sup>),  $A_{1g}^2$  (33.6 cm<sup>-1</sup>),  $E_g^1$  (107.9 cm<sup>-1</sup>), and  $A_{1g}^1$  (182.1 cm<sup>-1</sup>), respectively [28,29], where low-frequency shear  $E_g^2$  and breathing  $A_{1g}^2$  modes (in-plane and out-of-plane inter-layer relative motions) can hardly be resolved for few-layer samples. We define  $\theta$  as the rotated angle of the incident laser polarization from the initial parallel polarized configuration. For a clear view, we normalize four mode intensities by their maxima and plot the obtained values with respect to angle  $\theta$  in Fig. 2(b). Two  $E$  mode intensities are polarization insensitive whereas two  $A_{1g}$  modes have intensity oscillations of period  $\pi$ , showing the same symmetries of in-plane  $E$  and out-of-plane  $A_{1g}$  modes of MoS<sub>2</sub> [29,35–37]. Polarized Raman experiments indicate that  $E_g^1$  mode intensities rather than those of  $A_{1g}^1$  modes are more suitable for SnSe<sub>2</sub> thickness determination. The same  $E_g^1$  and  $A_{1g}^1$  mode intensity behaviors are obtained for one 3L SnSe<sub>2</sub> sample in Fig. 2(c). We then perform polarized Raman measurements using the 3L SnSe<sub>2</sub> sample without analyzer; the  $E_g^1$  mode intensity is still polarization insensitive, but the  $A_{1g}^1$  mode has an irregular intensity fluctuation with respect to  $\theta$ , which further supports that the intensity of  $E_g^1$  mode above 100 cm<sup>-1</sup> provides a convenient approach for thickness determination of SnSe<sub>2</sub> on SiO<sub>2</sub>/Si.

Temperature-dependent lattice vibrations of SnSe<sub>2</sub> are important for thermal property research such as thermal

conductivity, and 2D nano-optoelectronics performance. In Fig. 3, we present Raman spectra of 1L, 3L, and bulk SnSe<sub>2</sub> at a temperature range from 77 to 300 K. With decreasing temperature,  $E_g^1$  and  $A_{1g}^1$  modes of all samples blueshift with sharpened profiles, showing the general thermal effect of semiconductors. Within experimental error bars, the  $E_g^1$  and  $A_{1g}^1$  mode positions of three samples have a similar linear temperature dependence as shown in Figs. 4(a) and 4(b). From 77 to 300 K, the linear fitting procedure to obtain temperature coefficients has been widely used for 2D materials including SnSe<sub>2</sub> nanosheets as well as mono- to few-layer MoS<sub>2</sub> samples [38,39]. The linear dependence of Raman shift with temperature is described by the formula  $f(T) = f_0 + \chi T$ , where  $f(T)$  and  $f_0$  are Raman frequencies at temperature  $T$  and 0 K. Temperature coefficients  $\chi$  of 1L, 3L, and bulk samples are -0.0171, -0.0188, and -0.018 cm<sup>-1</sup>/K for  $E_g^1$  mode and -0.0138, -0.0137, and -0.0146 cm<sup>-1</sup>/K for  $A_{1g}^1$  mode, respectively.  $\chi$  values of  $A_{1g}^1$  mode are close to those of SnSe<sub>2</sub> nanosheets of -0.0129 cm<sup>-1</sup>/K [24] and -0.016 cm<sup>-1</sup>/K [40], comparable to those of mono- and few-layer MoS<sub>2</sub> as -0.016 and -0.011 cm<sup>-1</sup>/K [38,39].  $\chi$  values of  $E_g^1$  mode are also close to those of  $A_{1g}^1$  modes, similar to those of MoS<sub>2</sub>. One recent  $\chi$  value of the SnSe<sub>2</sub>  $E_g^1$  mode is -0.006 cm<sup>-1</sup>/K, where few-layer nanosheet samples were fabricated by the one-step solvothermal route [40]. Mechanical exfoliated single crystals used in our measurements could be the reason for this

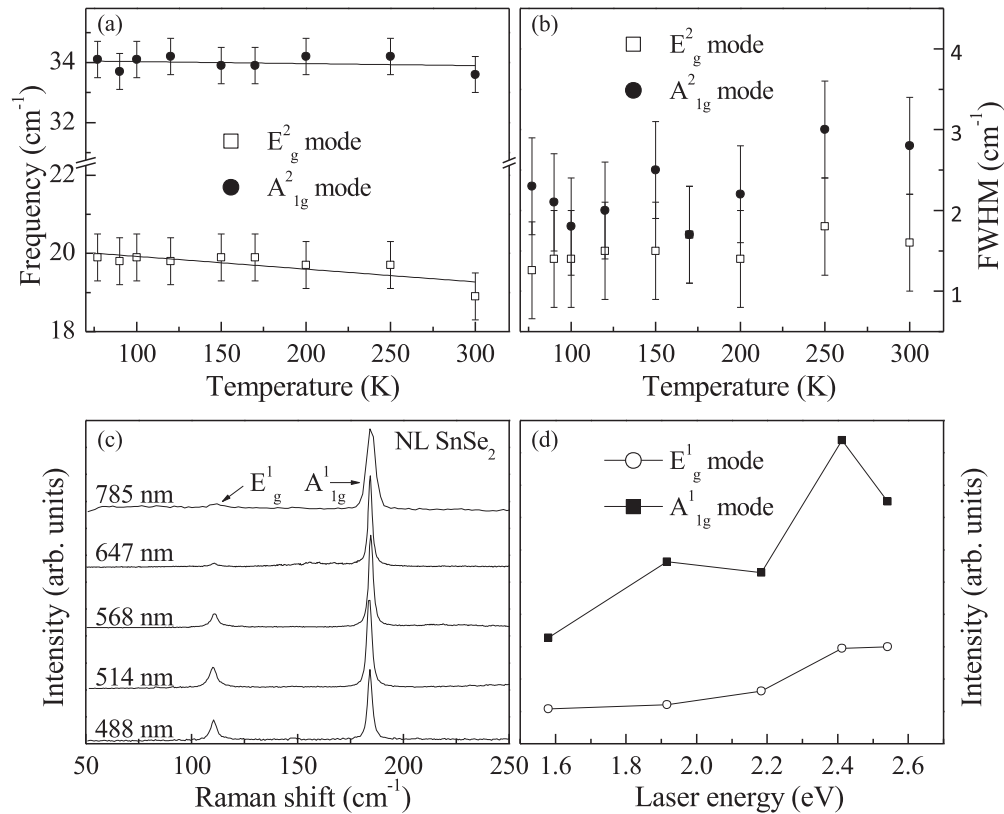


FIG. 5. (a) Raman shifts and (b) FWHM of low-frequency  $E_g^2$  (vacant squares) and  $A_{1g}^2$  (filled circles) modes with respect to temperature for bulk SnSe<sub>2</sub>. Solid lines are linear fittings of data. (c) Raman spectra of bulk SnSe<sub>2</sub> using excitation laser lines of 488, 514.5, 568, 647, and 785 nm. (d) Laser power normalized intensities of  $A_{1g}^1$  and  $E_g^1$  modes with respect to excitation laser energy. Lines connecting data points are a guide for the eye.

difference. In Figs. 4(c) and 4(d), full width at half maximum (FWHM) of three SnSe<sub>2</sub> samples all decrease with decreasing temperature almost linearly with slopes surprisingly smaller than those of peak positions. However, FWHM values of 1L SnSe<sub>2</sub> are larger than those of 3L and bulk samples for both  $E_g^1$  and  $A_{1g}^1$  modes, indicating a phonon scattering effect from the substrate, similar to few-layer black phosphorus [41]. For 3L and bulk SnSe<sub>2</sub> samples, FWHM of  $E_g^1$  and  $A_{1g}^1$  modes are both smaller than those of nanosheets [40], which shows the high quality of the mechanically exfoliated single crystal samples.

In Figs. 5(a) and 5(b), we present bulk SnSe<sub>2</sub> low-frequency  $E_g^2$  and  $A_{1g}^2$  mode shifts and FWHM with respect to temperature. The linear fitting gives temperature coefficients almost zero values (one to two orders smaller than those of  $E_g^1$  and  $A_{1g}^1$  modes), and the corresponding FWHM of no clear temperature trend, consistent with one previous observation [28]. Also different from the  $E_g^1$  and  $A_{1g}^1$  modes, the  $E_g^2$  mode becomes stronger with increasing temperature, which indicates in-plane rigid-layer vibrations increase with temperature, similar to the  $E_g^2$  mode behavior of MoS<sub>2</sub> [42].  $A_{1g}^1$  mode intensity is almost invariant, showing out-of-plane interlayer vibrations are quite insensitive to temperature. The different thermal behavior of interlayer and intralayer lattice vibrations can be useful in designing 2D devices.

Finally, we perform Raman measurements of bulk SnSe<sub>2</sub> using multiple excitation lasers (488, 514, 568, 647, and 785 nm) at room temperature. The indirect band gap of bulk SnSe<sub>2</sub> is around 1.0 eV, generally not accessible by lasers used in Raman experiments. In Fig. 5(c), Raman spectra above 50 cm<sup>-1</sup> are presented:  $E_g^1$  and  $A_{1g}^1$  modes are both nondispersive; their intensities are normalized by the incident laser power and plotted with respect to laser energy in Fig. 5(d). The normalized mode intensities have similar behavior and reach weak maxima at 2.41 eV, which could be from interband transitions. Different from resonant Raman scattering of TMDCs (including few-layer to bulk TMDCs of indirect band gaps) [43–47], where laser energies larger than band gaps lead to mode intensity resonances as well as second-order combination or overtone Raman modes, SnSe<sub>2</sub> has no clear resonant Raman modes and excitons (using a 488-nm laser) observed. Recently, to understand Raman intensity with respect to incident laser energy for 1L and 3L MoTe<sub>2</sub>, first-principles calculations have shown quantum interference and electron-phonon coupling contributions from

different electronic transitions of the Brillouin zone can be constructive or destructive, and excitonic effects are also important to explain the Raman mode intensity ratios [48]. The relation between lattice vibrations and electronic and excitonic states of SnSe<sub>2</sub> thus deserves more work because of its fundamental importance.

#### IV. CONCLUSION

In conclusion, we have exfoliated mono- to few-layer 6Hb-SnSe<sub>2</sub> samples and investigated their lattice dynamics by low-wave-number, polarized, low-temperature, and varying wavelength Raman experiments. We obtain Raman active shear mode  $E_g^2$ , breathing mode  $A_{1g}^2$ , and intralayer  $E_g^1$  and  $A_{1g}^1$  modes of bulk SnSe<sub>2</sub> about 18.9, 33.6, 107.9, and 182.1 cm<sup>-1</sup> at 300 K. SnSe<sub>2</sub> in-plane  $E_g^1$  mode intensity is insensitive to incident laser polarization and increases almost linearly with layer number, providing a convenient approach for layer number determination.  $E_g^1$  and  $A_{1g}^1$  mode frequency separation has no clear thickness dependence like MoS<sub>2</sub>, indicating a different type of interlayer coupling of SnSe<sub>2</sub>. We obtain temperature coefficients of  $E_g^1$  and  $A_{1g}^1$  modes about -0.018 and -0.014 cm<sup>-1</sup>/K, comparable to those of MoS<sub>2</sub>; for  $E_g^2$  and  $A_{1g}^2$  modes, Raman shifts and FWHM are both insensitive to temperature due to their interlayer nature. Multiple wavelength Raman measurements show  $E_g^1$  and  $A_{1g}^1$  modes have only weak intensity maxima for a 2.41-eV laser. Our investigation of SnSe<sub>2</sub> provides useful information for not only fundamental research, but also potential applications in the emerging thermal and optoelectronic 2D devices of atomic thickness.

#### ACKNOWLEDGMENTS

W.Z. acknowledges facility use from Prof. Miao Feng of the Physics Department of Nanjing University. This work was supported by the National Natural Science Foundation of China (61575129), NSAF (Grant No. U1530402) and the Shenzhen Science and Technology Project (JCYJ20140418091413577). L.W. acknowledges the Program for New Century Excellent Talents in University (NCET-10-0444) and the “Science Challenging Program.”

W.Z. and Z.Y. contributed equally to this work.

- 
- [1] K. S. Novoselov, D. Jiang, F. Schedin, T. J. Booth, V. V. Khotkevich, S. V. Morozov, and A. K. Geim, *Proc. Natl. Acad. Sci. USA* **102**, 10451 (2005).
  - [2] A. H. Castro Neto, F. Guinea, N. M. R. Peres, K. S. Novoselov, and A. K. Geim, *Rev. Mod. Phys.* **81**, 109 (2009).
  - [3] M. Chhowalla, H. S. Shin, G. Eda, L. J. Li, K. P. Loh, and H. Zhang, *Nat. Chem.* **5**, 263 (2013).
  - [4] Y. Liu, O. N. Weiss, X. D. Duan, H. C. Cheng, Y. Huang, and X. F. Duan, *Nat. Rev. Mater.* **1**, 16042 (2016).
  - [5] A. K. Geim and I. V. Grigorieva, *Nature* **499**, 419 (2013).
  - [6] D. Jariwala, V. K. Sangwan, L. J. Lauhon, T. J. Marks, and M. C. Hersam, *ACS Nano* **8**, 1102 (2014).
  - [7] H. Zhang, *ACS Nano* **9**, 9451 (2015).
  - [8] G. Fiori, F. Bonaccorso, G. Iannaccone, T. Palacios, D. Neumaier, A. Seabaugh, S. K. Banerjee, and L. Colombo, *Nat. Nanotechnol.* **9**, 768 (2013).
  - [9] C. Julien, M. Eddrief, I. Samaras, and M. Balkanski, *Mater. Sci. Eng., B* **15**, 70 (1992).
  - [10] B. Z. Sun, Z. Ma, C. He, and K. Wu, *Phys. Chem. Chem. Phys.* **17**, 29844 (2015).
  - [11] A. A. Kozma, Y. M. Sabov, Y. E. Peresh, E. I. Barchiy, and V. V. Tsyggyka, *Inorg. Mater.* **51**, 93 (2015).
  - [12] Y. Su, M. A. Ebrish, E. J. Olson, and S. J. Koester, *Appl. Phys. Lett.* **103**, 263104 (2013).

- [13] T. Pei, L. Bao, G. Wang, R. Ma, H. Yang, J. Li, C. Gu, S. Pantelides, S. Du, and H. J. Gao, *Appl. Phys. Lett.* **108**, 053506 (2016).
- [14] C. Guo, Z. Tian, Y. Xiao, Q. Mi, and J. Xue, *Appl. Phys. Lett.* **109**, 203104 (2016).
- [15] T. Roy, M. Tosun, M. Hettick, G. H. Ahn, C. Hu, and A. Javey, *Appl. Phys. Lett.* **108**, 083111 (2016).
- [16] R. Y. Wang, M. A. Caldwell, R. G. D. Jeyasignh, S. Aloni, R. M. Shelby, H. S. P. Wong, and D. J. Milliron, *J. Appl. Phys.* **109**, 113506 (2011).
- [17] K. M. Chung, D. Wamwangi, M. Woda, M. Wuttig, and W. Bensch, *J. Appl. Phys.* **103**, 083523 (2008).
- [18] X. Zhou, L. Gan, W. Tian, Q. Zhang, S. Jin, H. Li, Y. Bando, D. Golberg, and T. Zhai, *Adv. Mater.* **27**, 8035 (2015).
- [19] P. Yu, X. Yu, W. Lu, H. Lin, L. Sun, K. Du, F. Liu, W. Fu, Q. Zeng, Z. Shen, C. Jin, Q. Wang, and Z. Liu, *Adv. Funct. Mater.* **26**, 137 (2016).
- [20] X. Zhou, Q. Zhang, L. Gan, J. Xiong, and T. Zhai, *Adv. Sci.* **3**, 1600177 (2016).
- [21] R. Yan, S. Fathipour, Y. Han, B. Song, S. Xiao, M. Li, N. Ma, V. Protasenko, D. A. Muller, D. Jena, and H. G. Xing, *Nano Lett.* **15**, 5791 (2015).
- [22] J. M. Gonzalez and I. I. Oleynik, *Phys. Rev. B* **94**, 125443 (2016).
- [23] S. V. Bhatt, M. P. Deshpande, V. Sathe, and S. H. Chaki, *Solid State Commun.* **201**, 54 (2015).
- [24] A. Taube, A. Łapińska, J. Judek, and M. Zdrojek, *Appl. Phys. Lett.* **107**, 013105 (2015).
- [25] J. B. Renucci, R. N. Tyte, and M. Cardona, *Phys. Rev. B* **11**, 3885 (1975).
- [26] R. Schlaf, N. R. Armstrong, B. A. Parkinson, C. Pettenkofer, and W. Jaegermann, *Surf. Sci.* **385**, 1 (1997).
- [27] Y. Huang, E. Sutter, J. T. Sadowski, M. Cotlet, O. L. A. Monti, D. A. Racke, M. R. Neupane, D. Wickramaratne, R. K. Lake, B. A. Parkinson, and P. Sutter, *ACS Nano* **8**, 10743 (2014).
- [28] A. J. Smith, P. E. Meek, and W. Y. Liang, *J. Phys. C: Solid State Phys.* **10**, 1321 (1977).
- [29] X. Zhang, Q. H. Tan, J. B. Wu, W. Shi, and P. H. Tan, *Nanoscale* **8**, 6435 (2016).
- [30] S. Tongay, H. Sahin, C. Ko, A. Luce, W. Fan, K. Liu, J. Zhou, Y. S. Huang, C. H. Ho, J. Y. Yan, D. F. Ogletree, S. Aloni, J. Ji., S. S. Li, J. B. Li, F. M. Peeters, and J. Q. Wu, *Nat. Commun.* **5**, 3252 (2014).
- [31] X. Luo, Y. Zhao, J. Zhang, Q. Xiong, and S. Y. Quek, *Phys. Rev. B* **88**, 075320 (2013).
- [32] G. Froehlicher, E. Lorchat, F. Fernique, C. Joshi, A. Molina-Sánchez, L. Wirtz, and S. Berciaud, *Nano Lett.* **15**, 6481 (2015).
- [33] E. Lorchat, G. Froehlicher, and S. Berciaud, *ACS Nano* **10**, 2752 (2016).
- [34] S. L. Li, H. Miyazaki, H. Song, H. Kuramochi, S. Nakaharai, and K. Tsukagoshi, *ACS Nano* **6**, 7381 (2012).
- [35] Y. Wang, C. Cong, C. Qiu, and T. Yu, *Small* **9**, 2857 (2013).
- [36] X. Zhang, W. P. Han, J. B. Wu, S. Milana, Y. Lu, Q. Q. Li, A. C. Ferrari, and P. H. Tan, *Phys. Rev. B* **87**, 115413 (2013).
- [37] X. Zhang, X. F. Qiao, W. Shi, J. B. Wu, D. S. Jiang, and P. H. Tan, *Chem. Soc. Rev.* **44**, 2757 (2015).
- [38] N. A. Lanzillo, A. G. Birdwell, M. Amani, F. J. Crowne, P. B. Shah, S. Najmaei, Z. Liu, P. M. Ajayan, J. Lou, M. Dubey, S. K. Nayak, and T. P. O'Regan, *Appl. Phys. Lett.* **103**, 093102 (2013).
- [39] M. Thirupuranthaka, R. V. Kashid, C. S. Rout, and D. J. Late, *Appl. Phys. Lett.* **104**, 081911 (2014).
- [40] A. S. Pawbake, S. R. Jadhkar, and D. J. Late, *ChemistrySelect* **1**, 5380 (2016).
- [41] L. Q. Su and Z. Yong, *Appl. Phys. Lett.* **107**, 071905 (2015).
- [42] S. Sahoo, A. P. Gaur, M. Ahmadi, M. J. F. Guinel, and R. S. Katiyar, *J. Phys. Chem. C* **117**, 9042 (2013).
- [43] B. R. Carvalho, L. M. Malard, J. M. Alves, C. Fantini, and M. A. Pimenta, *Phys. Rev. Lett.* **114**, 136403 (2015).
- [44] P. Soubelet, A. E. Bruchhausen, A. Fainstein, K. Nogajewski, and C. Faugeras, *Phys. Rev. B* **93**, 155407 (2016).
- [45] E. Del Corro, H. Terrones, A. Elias, C. Fantini, S. Feng, M. A. Nguyen, T. E. Mallouk, M. Terrones, and M. A. Pimenta, *ACS Nano* **8**, 9629 (2014).
- [46] R. Saito, A. R. Nugraha, E. H. Hasdeo, S. Siregar, H. Guo, and T. Yang, *Phys. Status Solidi B* **252**, 2363 (2015).
- [47] Q. J. Song, Q. H. Tan, X. Zhang, J. B. Wu, B. W. Sheng, Y. Wan, X. Q. Wang, L. Dai, and P. H. Tan, *Phys. Rev. B* **93**, 115409 (2016).
- [48] H. P. Miranda, S. Reichardt, G. Froehlicher, A. Molina-Sánchez, S. Berciaud, and L. Wirtz, *Nano Lett.* **17**, 2381 (2017).